

Accurate $^{238}\text{U}(n, 2n)^{237}\text{U}$ reaction cross-section measurements from 6.5 to 14.8 MeVKrishichayan,^{1,2,*} M. Bhike,^{1,2} W. Tornow,^{1,2} A. P. Tonchev,³ and T. Kawano⁴¹*Department of Physics, Duke University, Durham, North Carolina 27708, USA*²*Triangle Universities Nuclear Laboratory, Durham, North Carolina 27708, USA*³*Nuclear and Chemical Sciences Division, Lawrence Livermore National Laboratory, Livermore, California 94550, USA*⁴*Los Alamos National Laboratory, Los Alamos, New Mexico 87545, USA*

(Received 5 September 2017; published 26 October 2017)

The cross section for the $^{238}\text{U}(n, 2n)^{237}\text{U}$ reaction has been measured in the incident neutron energy range from 6.5 to 14.8 MeV in small energy steps using an activation technique. Monoenergetic neutron beams were produced via the $^2\text{H}(d, n)^3\text{He}$ and $^3\text{H}(d, n)^4\text{He}$ reactions. ^{238}U targets were activated along with Au and Al monitor foils to determine the incident neutron flux. The activity of the reaction products was measured in TUNL's low-background counting facility using high-resolution γ -ray spectroscopy. The results are compared with previous measurements and latest data evaluations. Statistical-model calculations, based on the Hauser-Feshbach formalism, have been carried out using the CoH₃ code and are compared with the experimental results. The present self-consistent and high-quality data are important for stockpile stewardship and nuclear forensic purposes as well as for the design and operation of fast reactors.

DOI: [10.1103/PhysRevC.96.044623](https://doi.org/10.1103/PhysRevC.96.044623)**I. INTRODUCTION**

The $^{238}\text{U}(n, 2n)^{237}\text{U}$ reaction cross section constitutes a significant part of the nonelastic reactions on ^{238}U at neutron energies above 6.0 MeV. These energies correspond to a region where the fission (n, f) cross section exhibits a step-function-like increase, and where the fission channel and the ($n, 2n$) reaction are dominant compared with other competing neutron-induced processes, such as neutron capture (n, γ) and inelastic neutron scattering (n, n') [1]. Because both fission and ($n, 2n$) reaction channels compete at neutron energies above 6 MeV, the absolute magnitude of these cross sections is of primary importance for stockpile stewardship and nuclear forensic as well as safety assessment of fast reactors [2,3].

As an important flux monitor for high-energy neutrons, the excitation function of the $^{238}\text{U}(n, 2n)^{237}\text{U}$ reaction has been measured by many authors, using either the activation methods, the spherical shell technique, or neutron spectroscopy [4–27]. Besides the experimental data in the EXFOR library of the NNDC webpage [28], evaluated data of the $^{238}\text{U}(n, 2n)^{237}\text{U}$ reaction cross section over a wide range of neutron energies are available from different compilations, e.g., ENDF/B-VIII.b4, JENDL-4.0, JEFF-3.2, CENDL-3.1, BROND-2.2, Zhou You-Pu, Zolotarev [28,29].

Despite continued effort for several decades, there still lacks a comprehensive and self-consistent measurement of the $^{238}\text{U}(n, 2n)^{237}\text{U}$ reaction cross section over a broad energy range with small uncertainties, plus a detailed comparison of the measured cross-section data with the results of statistical-model calculations and the latest data evaluations. In this article, we describe an activation based measurement of the $^{238}\text{U}(n, 2n)^{237}\text{U}$ reaction cross section in order to provide an accurate data set for evaluators and simulation codes. Monoenergetic neutron beams with high flux, pure/background-less

activation targets, and high-resolution γ -ray spectroscopy techniques have helped minimize the uncertainties of the measurements.

II. EXPERIMENTAL DETAILS

The neutron activation of ^{238}U was carried at the 10-MV FN Tandem Accelerator of the Triangle Universities Nuclear Laboratory (TUNL) [30]. The measurements were performed in the so-called neutron time-of-flight (NTOF) room, a large 10×16 m room with high ceilings, which helps to reduce the effect of room return neutrons at the position of the activation target.

Quasi-monoenergetic neutron beams were produced via the $^2\text{H}(d, n)^3\text{He}$ and $^3\text{H}(d, n)^4\text{He}$ reactions. Relevant information about each of these reactions is given in Table I of Ref. [31]. The $^2\text{H}(d, n)^3\text{He}$ reaction with its positive Q value and its large cross section is the most commonly used neutron production reaction in the 5 to 13 MeV energy range. Deuterium gas was contained in a 3-cm-long cylindrical cell with pressures adjusted in the 2 to 4 atm range to keep the neutron energy spread below ± 200 keV (FWHM). The cell was sealed from the beam line vacuum by a $6.35 \mu\text{m}$ thin Havar foil [31]. The pressure in the gas cell and the energy straggling of the deuteron beam in the Havar foil contributed to the energy spread of the neutron beam. The deuteron energy loss was calculated using the program MAGNET [30] with the incident deuteron beam energy, the length of the gas cell, the deuterium gas pressure, the thickness of the Havar foil, and the ambient temperature as inputs. Typical deuteron beam currents on target were $\sim 2 \mu\text{A}$. The $^3\text{H}(d, n)^4\text{He}$ reaction is the favored reaction for neutron production in the 14 MeV energy region. This reaction was used for our three measurements at neutron energies of $E_n = 13.6, 14.1, \text{ and } 14.8$ MeV. A $3.8 \text{ cm} \times 3.8 \text{ cm}$ BC-501A based neutron detector [32] was placed at 0° relative to the incident deuteron beam. During irradiation, the neutron detector operated in the multichannel-scaling acquisition mode

*krishi@tunl.duke.edu; krishichayan@gmail.com

TABLE I. Information on the ^{238}U targets and Al and Au monitor foils used in the present measurements. All targets and monitor foils were of 1.27 cm diameter. The ^{238}U targets were depleted to the 99.97% level, whereas the natural monitor foils were of 99.999% purity.

Target	Mass (mg)
^{238}U (ID #)	
old	441.93(60)
109	172.55(20)
110	242.60(20)
111	240.79(20)
112	236.56(20)
113	260.70(30)
^{197}Au foils	120.5(1)–131.34(1)
^{27}Al foils	16.87(1)–19.14(2)

to record the time profile of the neutron flux, allowing us to make off-line corrections for any beam current variation. A total of six 1.27 cm diameter and depleted ^{238}U targets were used during the course of our measurements. They were mounted normal to the incident beam at a distance of 2.54 cm downstream from the end of the deuterium gas cell when the $^2\text{H}(d,n)^3\text{He}$ reaction was employed. For the measurements with the $^3\text{H}(d,n)^4\text{He}$ reaction the tritiated target described in Ref. [33] was used to produce 14.8 MeV neutrons at 0° , and 13.6 MeV neutrons at 135° . The ^{238}U target was positioned at a distance of 2.54 cm from the 0.4 mm thick Cu backing of the tritiated titanium foil. A special tritiated target cell had to be used at 14.1 MeV in order to minimize the scattering of neutrons from structural materials before they interact with the ^{238}U target. Here, the tritiated titanium foil was mounted at a 45° angle relative to the incident deuteron beam, with the ^{238}U target mounted at 90° . The ^{238}U targets were sandwiched between natural Al/Au foils of the same diameter in order to determine the neutron fluence incident on the targets. Table I provides information on the properties of the ^{238}U and monitor foils. The depleted ^{238}U targets were provided by Los Alamos National Laboratory. The mass of these targets is determined by weighing. Afterwards, the targets were sealed with mylar tape to prevent oxidation and/or loss of material during irradiation.

During 20 experimental runs, the ^{238}U targets were irradiated at 16 different neutron energies [$E_n = 6.34(0.21)$, $6.89(0.20)$, $7.40(0.19)$, $7.87(0.25)$, $8.38(0.24)$, $8.89(0.23)$, $9.40(0.23)$, $9.91(0.21)$, $10.41(0.21)$, $10.92(0.17)$, $11.42(0.18)$, $11.93(0.18)$, $12.43(0.18)$, $13.60(0.06)$, $14.1(0.06)$, and $14.8(0.06)$ MeV], where the numbers in parentheses represent the energy spread (FWHM) in MeV of the neutron beam. Because of kinematics, the off- 0° neutrons have a lower energy than the neutrons emitted parallel to the deuteron beam. This kinematic effect was taken into account via Monte Carlo simulation by using the angular distribution of the neutron flux across the width of the targets, the differential cross-section data of the $^2\text{H}(d,n)^3\text{He}$ reaction [34], and the deuteron energy loss along the length of the gas cell. As an example, for 12.5 MeV neutrons produced at the center of the gas cell, the energy

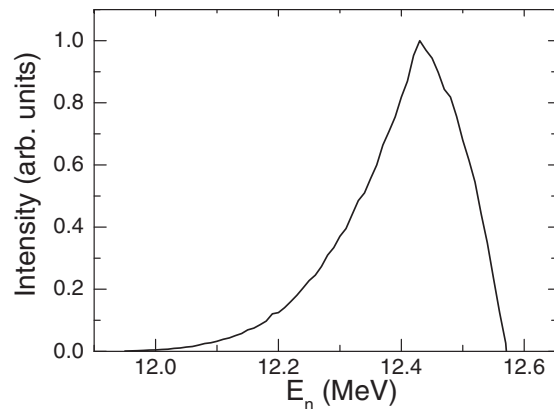


FIG. 1. Calculated energy distribution of neutrons hitting the ^{238}U target at the 12.5-MeV settings. The spread in neutron energies is primarily caused by kinematic effects due to the extended geometry of the deuterium gas cell and the target sample.

distribution of the neutrons hitting the foils is shown in Fig. 1. The spread of the neutron energy distribution at other settings is similar in shape, except for the data taken with the $^3\text{H}(d,n)^4\text{He}$ reaction, where the neutron energy distribution is more narrow, as expected from the 2 mg/cm^2 titanium layer loaded with 74 GBq of tritium.

The ^{238}U targets along with the monitor foils were irradiated for 1.5 to 9 h depending on the neutron beam energy and the corresponding $(n,2n)$ reaction cross section. Neutrons from the deuteron breakup on structural materials of the deuterium gas cell have energies below the $^{238}\text{U}(n,2n)^{237}\text{U}$ reaction threshold as long as the $^2\text{H}(d,n)^3\text{He}$ neutrons do not exceed an energy of 11.5 MeV. Therefore, small corrections had to be applied to the data obtained at 11.93 and 12.43 MeV. ^{238}U activation data obtained with the deuterium gas pumped out of the gas cell provide an experimental determination of the “break-up” neutron contribution to the cross section of interest. The $^{197}\text{Au}(n,2n)^{196}\text{Au}$ reaction with its threshold of 8.11 MeV is not sensitive to any break-up neutrons for the deuteron energies used in the present work. Neutrons from the deuteron breakup on the deuterium gas itself are below the $^{238}\text{U}(n,2n)^{237}\text{U}$ threshold and therefore, do not contribute in the deuteron energy range used in the present analysis.

Following the irradiation, the targets were γ -ray counted in TUNL’s low-background counting facility, using a set of high efficient standard HPGe and HPGe Clover detectors. These detectors are elaborately lead-shielded against room and cosmic-ray background radiations. The irradiated targets were placed in plastic (acrylic) containers and positioned at a distance of 5 cm from the front face of the respective detectors throughout the measurements. The dead time of the counting system was less than 1%. Over a period of 1–2 months, the targets were measured using a number of different counting cycles, depending on the half-lives of the product nuclei. A Canberra Multiport II multichannel analyzer was used for the data-acquisition system and spectra were accumulated using the GENIE-2000 software [35] with active pile-up rejection.

Because the photopeak count rate in the γ -ray spectrum is used to determine the activity of the target, the efficiency

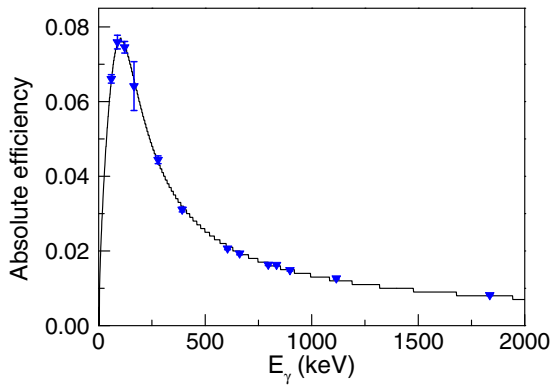


FIG. 2. Measured absolute efficiency for a HPGe Clover detector (sum of all four crystals) using a mixed nuclide γ -ray source. The solid curve is the fit to the data values (see text for details). A large error associated with the 165.8 keV γ ray is due to the error in the measured intensity data ($\sim 10\%$ [28]).

of each detector was determined accurately using a mixed nuclide γ -ray source (obtained from Eckert and Ziegler [36]) under identical conditions as those used for counting the ^{238}U targets and monitor foils. Mixed γ -ray sources are useful since a number of energies (ranging from 59.54 to 1836.06 keV) can be measured simultaneously rather than repeating efficiency measurements for separate sources. Because the majority of the nuclides in the mixed source are single γ -ray emitters and therefore, are not in coincidence with any other transitions, coincidence summing effects are practically eliminated. Figure 2 shows the efficiency curve for the HPGe Clover detector. The program “effit” from the RADWARE package [37] was used to fit the individual efficiency data values.

III. DATA ANALYSIS

The acquired γ -ray spectra from the off-line measurements of the activated targets were analyzed to identify the reaction products and to determine the respective peak areas using the GF3 package of the RADWARE software [37]. Typical γ -ray spectra (of the region of interest) from the $^{238}\text{U}(n,2n)^{237}\text{U}$, $^{27}\text{Al}(n,\alpha)^{24}\text{Na}$, and $^{197}\text{Au}(n,2n)^{196}\text{Au}$ reactions are shown in Figs. 3 and 4. The top panel of Fig. 3 shows the spectrum obtained from the target ^{238}U before irradiation. As can be seen, the region of interest ($E_\gamma = 208.01$ keV) for the $^{238}\text{U}(n,2n)^{237}\text{U}$ reaction is not contaminated with background lines. The ^{27}Al and ^{197}Au monitor foils were never irradiated before. Table II lists the different reaction channels studied in the present measurements along with the primary γ lines used for identifying isotopes as well as the corresponding intensities and the product half-lives. The half-lives of the products from the $^{238}\text{U}(n,2n)^{237}\text{U}$, $^{197}\text{Au}(n,2n)^{196}\text{Au}$, and $^{27}\text{Al}(n,\alpha)^{24}\text{Na}$ reactions were determined from the cycle measurements of the activated targets and compared to the adopted values. Decay curves for $^{238}\text{U}(n,2n)^{237}\text{U}$, $^{197}\text{Au}(n,2n)^{196}\text{Au}$, and $^{27}\text{Al}(n,\alpha)^{24}\text{Na}$ are illustrated in Fig. 5. The associated half-life times are in very good agreement with the literature values from the National Nuclear Data Center database [28]. The incident neutron

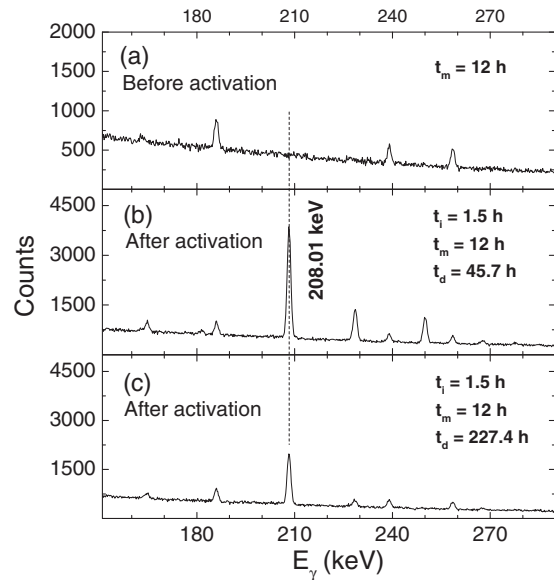


FIG. 3. γ -ray spectra measured before (a) and after activation [(b) and (c)] of the ^{238}U target with $E_n = 10.5$ MeV neutrons. The decay of ^{237}U associated with the γ -ray line at 208.01 keV is shown at two different decay times. The activation conditions (irradiation, measurement, and decay times) are also given.

flux and the reaction cross section for $^{238}\text{U}(n,2n)^{237}\text{U}$ was calculated from the well-known activation formula [38–40]

$$A = \sigma \phi n (1 - e^{-\lambda t_i}) e^{-\lambda t_d} (1 - e^{-\lambda t_m}), \quad (1)$$

where A is the induced activity, σ is the cross section, ϕ is the incident flux, n is the number of target nuclei, λ is the decay constant, and t_i , t_d , t_m , are the irradiation, decay, and measurement times, respectively.

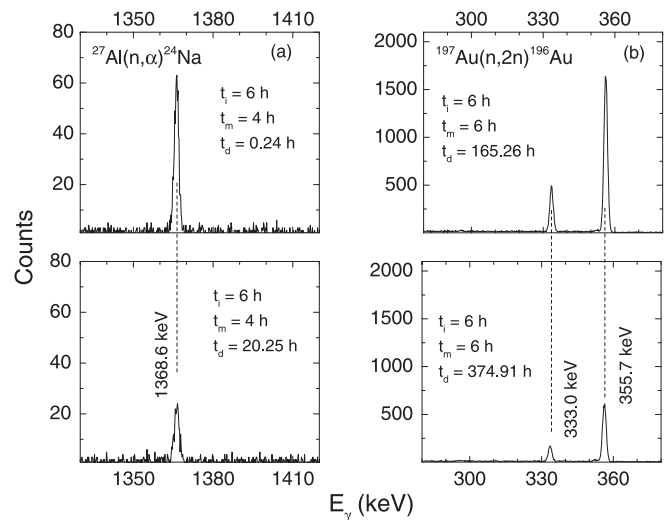


FIG. 4. γ -ray spectra measured after activation of the ^{27}Al (a) and ^{197}Au (b) monitor foils with $E_n = 6.5$ and 13.6 MeV, respectively, are shown at two different times (top and bottom). The characteristic γ -ray lines are indicated. The vertical dash lines are for guiding purposes only. The activation conditions (irradiation, measurement, and decay times) are also given.

TABLE II. Decay data for nuclear reactions used in the present work [28].

Reaction	Q value (MeV)	Product half-life	E_γ (keV)	I_γ
$^{238}\text{U}(n,2n)^{237}\text{U}$	-6.1543(1)	6.75(1) d	208.01(2)	0.212(3)
$^{197}\text{Au}(n,2n)^{196}\text{Au}$	-8.072(2)	6.1669(6) d	355.73(5)	0.87
$^{27}\text{Al}(n,\alpha)^{24}\text{Na}$	-3.1324(1)	14.997(12) h	1368.63(5)	0.9999(1)

and measurement times, respectively. The induced activity is obtained from the peak area of the respective γ -ray transition, normalized by the corresponding intensity, the disintegration rate of the radioactive product, and the efficiency of the detector.

One of the key ingredients in determining the cross section from the measured data is the incident neutron flux. In the present measurements the incident flux was obtained from the monitor reactions on ^{197}Au and ^{27}Al foils irradiated along with the ^{238}U targets. The required cross-section values for the $^{197}\text{Au}(n,2n)$ and $^{27}\text{Al}(n,\alpha)$ reactions needed in the activation formula were taken from the work of Zolotarev [41,42]. Because the threshold for the ^{197}Au monitor reaction is 8.11 MeV, the flux at neutron mean energy lower than 10.0 MeV was determined using ^{27}Al monitor foils. For each given neutron energy, the standard cross-section value was obtained by linear interpolation of the tabulated data given in Refs. [41,42].

IV. RESULTS AND DISCUSSION

Using the measured 208.01 keV ^{237}U γ -ray line yields with the calibrated γ -ray efficiency, neutron fluence determinations obtained from the monitor foil yields and monitor reaction cross sections, target thickness assay, and decay scheme information, the $^{238}\text{U}(n,2n)^{237}\text{U}$ cross-section value was calculated for each neutron irradiation. The cross-section data obtained in the incident neutron energy range from 6.5 to 14.8 MeV are tabulated in Table III. Figure 6 shows the measured cross-section data as a function of incident neutron energy from 6 to 15 MeV, along with the data from the literature, as well the latest evaluations. As can be seen from Fig. 6, the experimental $^{238}\text{U}(n,2n)^{237}\text{U}$ reaction cross-section data have a rapidly increasing trend between neutron energies of 6.0 to 8.5 MeV. Above that energy range the slope remains almost constant up to 12.5 MeV and then drops above 13 MeV. This

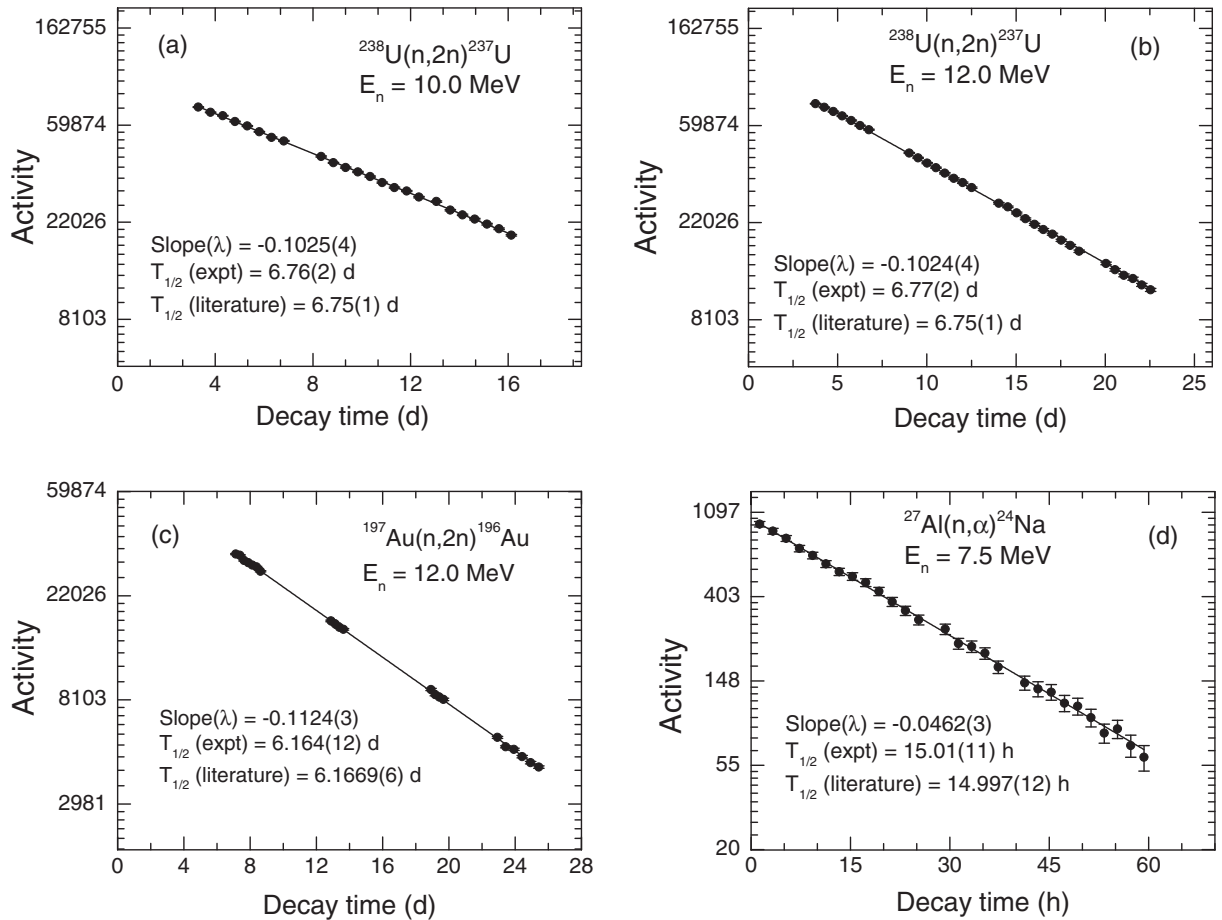


FIG. 5. Determination of half-lives of the activation products ^{237}U (a and b), ^{196}Au (c), and ^{24}Na (d). The γ -ray transitions used for these nuclei are listed in Table II. Note the logarithmic (base e) scales.

TABLE III. Cross-section values for $^{238}\text{U}(n,2n)^{237}\text{U}$ reaction measured in the present work at neutron energies from $E_n = 6.5$ to 14.8 MeV. Also given are the reaction cross-section data for the monitor reactions, taken from Refs. [41,42].

E_n (MeV)	$^{27}\text{Al}(n,\alpha)^{24}\text{Na}$ (mb)	$^{197}\text{Au}(n,2n)^{196}\text{Au}$ (b)	$^{238}\text{U}(n,2n)^{237}\text{U}$ (b)
6.34(21)	5.21(11)		0.07(1)
6.89(20)	15.05(23)		0.39(1)
7.40(19)	25.96(29)		0.82(1)
7.87(25)	38.07(34)		1.14(3)
8.38(24)	52.04(44)		1.27(3)
8.89(23)	66.03(59)		1.36(4)
9.40(23)	78.54(68)		1.37(3)
9.91(21)		0.97(3)	1.45(4)
10.41(21)		1.22(4)	1.42(3)
10.92(17)		1.42(4)	1.44(3)
11.42(18)		1.58(4)	1.44(4)
11.93(18)		1.71(4)	1.43(4)
12.43(18)		1.83(4)	1.40(4)
13.60(6)		2.09(3)	1.11(3)
14.10(6)		2.14(2)	0.89(2)
14.80(6)		2.16(2)	0.66(2)

variation in the excitation function can be attributed to the sharing of the excitation energy between different reaction channels, particularly $^{238}\text{U}(n,\gamma)$, $^{238}\text{U}(n,f)$, and $^{238}\text{U}(n,3n)$.

Since the 1950s a substantial amount of effort has been made to measure the $^{238}\text{U}(n,2n)^{237}\text{U}$ cross section. Table IV lists the previous measurements of the $^{238}\text{U}(n,2n)^{237}\text{U}$ reaction

cross section available in the literature [28] at neutron energies between 5 and 15 MeV. The first attempt (as per the NNDC EXFOR data library [28]) to measure the $^{238}\text{U}(n,2n)^{237}\text{U}$ cross section was carried out by Phillips *et al.* [4] in 1956 at $E_n = 14.1$ MeV, followed by a measurement at $E_n = 15.0$ MeV by Antropov *et al.* [5] in 1958. Since then many experimental groups around the world carried out $^{238}\text{U}(n,2n)^{237}\text{U}$ cross-section measurements in the $E_n \sim 14\text{--}15$ MeV region. The measurements of Knight *et al.* [6] performed in 1958 ($E_n = 6\text{--}10$ MeV) used the ratio of $(n,2n)/(n,f)$ measurements to calculate the $^{238}\text{U}(n,2n)^{237}\text{U}$ cross-section data, which relied on then available fission cross-section data. Mather *et al.* used a large loaded liquid scintillator to measure the cross section at $E_n = 7, 8, 12.4,$ and 14.06 MeV. $^{238}\text{U}(n,f)$ was used as a monitor reaction. In 1980, three groups reported $^{238}\text{U}(n,2n)^{237}\text{U}$ cross-section data in the energy range of $E_n = 6\text{--}15$ MeV. The activation method was used by Kornilov *et al.* [13] and Raics *et al.* [16]. Similar to the approach by Mather *et al.*, Frehaut *et al.* [15] used a large gadolinium-loaded liquid scintillator to determine the $^{238}\text{U}(n,2n)^{237}\text{U}$ cross section. In recent years, Naik and his group [23–26] used the activation technique for the cross-section measurements at $E_n = 8.0, 10.0, 12.0, 14.8,$ and 15.5 MeV. Our present data are in good agreement with the values reported by Knight *et al.* [6] and Raics [16]. The cross-section values reported by Frehaut *et al.* are consistently lower and higher than our present data in the energy range of $E_n = 6\text{--}12$ and $E_n = 13\text{--}15$ MeV, respectively.

The ENDF/B-VIII.b4 evaluation is in very good agreement with the present measurements almost over the entire energy range. The JEFF-3.2 evaluation has very good overlap with the

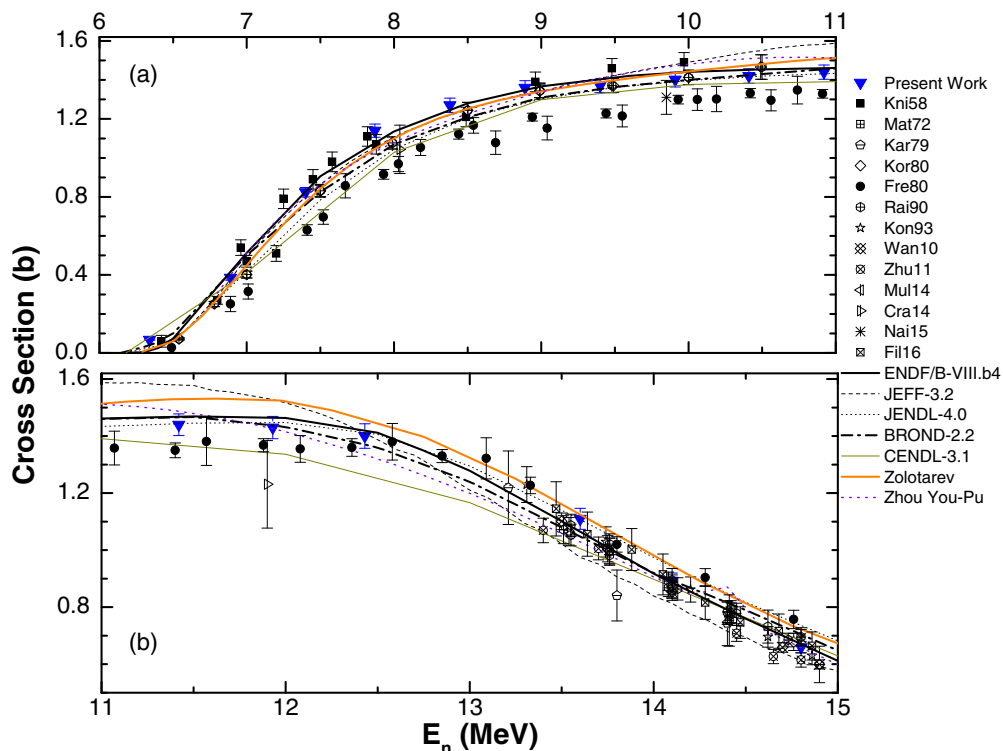


FIG. 6. Present experimental cross-section data (downward pointing triangle) for the $^{238}\text{U}(n,2n)^{237}\text{U}$ reaction are plotted as a function of incident neutron energy and shown in comparison to previous data from the literature as well as to the latest evaluations.

TABLE IV. Previous measurements of the $^{238}\text{U}(n,2n)^{237}\text{U}$ reaction cross section in the range of 6.0–15.0 MeV [28]. Information on the latest evaluation libraries is also given.

First author	Year	E_γ range (MeV)	Beam
Phillips [4]	1956	14.1	$^3\text{H}(d,n)^4\text{He}$
Antropov [5]	1958	15.0	$^3\text{H}(d,n)^4\text{He}$
Knight [6]	1958	5.98–9.97	$^2\text{H}(d,n)^3\text{He}$
Perkin [7]	1961	14.5	$^3\text{H}(d,n)^4\text{He}$
Mather [8]	1969	14.06	$^3\text{H}(d,n)^4\text{He}$
Mather [9]	1972	7.0, 8.0, 12.4	$^2\text{H}(d,n)^3\text{He}$ & $^3\text{H}(d,n)^4\text{He}$
Landrum [10]	1973	13.7–14.95	$^3\text{H}(d,n)^4\text{He}$
Veesser [11]	1878	14.7–19.0	$^3\text{H}(d,n)^4\text{He}$
Karius [12]	1979	13.2–18.1	$^3\text{H}(d,n)^4\text{He}$
Kornilov [13]	1980	6.5–14.76	$^2\text{H}(d,n)^3\text{He}$ & $^3\text{H}(d,n)^4\text{He}$
Ryves [14]	1980	14.68	$^3\text{H}(d,n)^4\text{He}$
Frehaut [15]	1980	6.49–14.76	$^2\text{H}(d,n)^3\text{He}$ & $^3\text{H}(d,n)^4\text{He}$
Raics [16]	1980	6.54–14.76	$^2\text{H}(d,n)^3\text{He}$ & $^3\text{H}(d,n)^4\text{He}$
Anders [17]	1986	14.7	$^3\text{H}(d,n)^4\text{He}$
Golovnya [18]	1987	14.76	$^3\text{H}(d,n)^4\text{He}$
Raics [19]	1990	13.51–14.8	$^3\text{H}(d,n)^4\text{He}$
Konno [20]	1993	13.3–14.9	$^3\text{H}(d,n)^4\text{He}$
Wang [21]	2010	13.5–14.9	$^3\text{H}(d,n)^4\text{He}$
Zhu [22]	2011	13.4–14.8	$^3\text{H}(d,n)^4\text{He}$
Naik [23]	2012	9.85	$^7\text{Li}(p,n)^7\text{Be}$
Crasta [24]	2014	8.04, 11.9	$^7\text{Li}(p,n)^7\text{Be}$
Mulik [25]	2014	15.5	$^7\text{Li}(p,n)^7\text{Be}$
Naik [26]	2015	14.8	$^3\text{H}(d,n)^4\text{He}$
Filatnikov [27]	2016	13.47–14.86	$^3\text{H}(d,n)^4\text{He}$
Evaluation libraries [28]			
Zhou You-Pu		1978	
ROSFOND-2010		2006	
CENDL-3.1		2009	
JEFF-3.2		2011	
JENDL-4.0		2012	
ENDF/B-VIII.b4		2014	
Zolotarev [29]		2017	

present measurements below 9 MeV, but continues to increase at higher energies up to 11.0 MeV, after which it follows a negative slope. The CENDL-3.1 evaluation has very poor agreement with the present data, but agrees quite well with the results of Frehaut *et al.* [15] up to $E_n = 12$ MeV. Zolotarev [29] has recently published his report on the latest evaluation of the $^{238}\text{U}(n,2n)^{237}\text{U}$ cross section. The Zolotarev evaluation is in close agreement with our data below 10.5 MeV, while it does not agree at higher energies except at $E_n = 13$ MeV. Figure 7 shows the variation of the evaluation data with respect to our data set. As can be seen, except for ENDF/B-VIII.b4, all other evaluation data sets have a positive slope at $E_n = 10$ –11.5 MeV, whereas the measured cross-section values are almost constant in this energy range.

V. THEORETICAL CALCULATIONS

We performed statistical Hauser-Feshbach model calculations for the neutron induced reactions on ^{238}U with the CoH₃ code [43], and compared the results with our measured data (see Fig. 8). CoH₃ combines the coupled-channels optical model and the statistical Hauser-Feshbach theory.

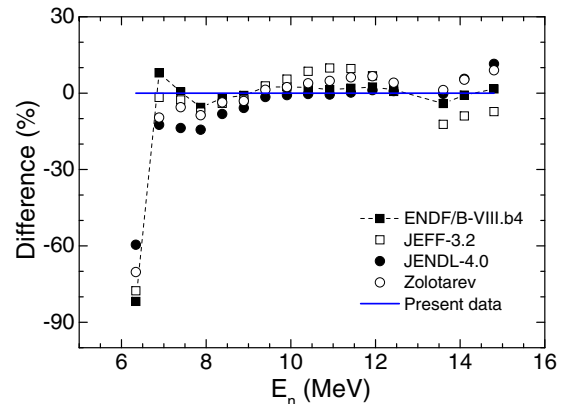


FIG. 7. Comparison of the present data to the data taken from the latest evaluations.

The direct cross sections to the coupled levels are correctly taken into account by applying the Engelbrecht-Weidenmüller transformation to the scattering matrix [44,45]. To avoid a convergence problem in the coupled-channels method [46], six states (0^+ , 2^+ , 4^+ , 6^+ , 8^+ , and 10^+) in the ground state rotational band are coupled. We adopt the optical potential of Soukhovitskii *et al.* [47], and the deformation parameters β_2 , β_4 and β_6 are taken from the finite-range droplet model (FRDM) [48]. For the other collective states, such as the octupole vibrational band levels, we employ the DWBA method to calculate the direct inelastic scattering cross section. The γ -ray transmission coefficient is calculated from the γ -ray strength functions. For the double-humped $E1$ strength we adopt the generalized Lorentzian form of Kopecky and Uhl [49]. For the higher multiplicities in the standard Lorentzian, information was taken from the parameter systematics in RIPL-3 [50]. We also consider the $M1$ scissors mode [51,52].

At the incident neutron energies of around 10 MeV, the total compound formation cross section, which is determined by the optical potential employed, is split into the (n, n') , $(n, 2n)$, first-chance fission (n, f) , and second chance fission $(n, n'f)$ channels. To calculate the $(n, 2n)$ cross section we have to pay attention not only to the neutron emission channel, but also

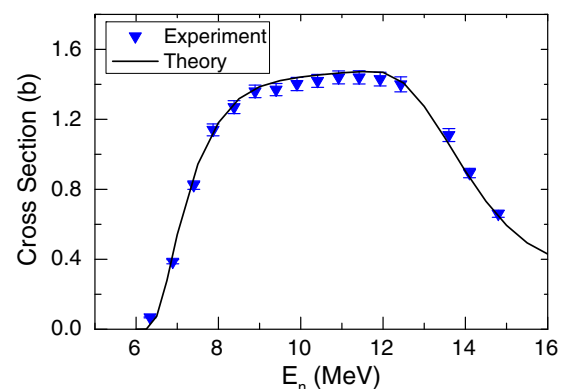


FIG. 8. Hauser-Feshbach model based theoretical calculation is compared to the experimental cross-section data for the $^{238}\text{U}(n,2n)^{237}\text{U}$ reaction.

the fission channel. Because the fission model in the Hauser-Feshbach code is still not as sophisticated as desirable, and the calculated fission cross section is very sensitive to the fission penetrabilities, prediction of the fission cross sections by the model itself is not very accurate. Here, we adjust the fission parameters (height and curvature of the fission barrier) to reproduce the evaluated fission cross section in ENDF/B-VII.1 [28]. This procedure gives us some confidence that the calculated neutron emission channels should be reasonable. As can be seen from Fig. 8, the calculations referred to above provide an almost excellent description of our data. In the 9 to 12 MeV energy range the data are half an error bar lower than the calculations.

VI. SUMMARY

This work presents an accurate and self-consistent set of high-quality cross-section data for the $^{238}\text{U}(n,2n)^{237}\text{U}$ reaction from 6.5 to 14.8 MeV. The data are important to issues pertaining to stockpile stewardship and nuclear forensics, as well as the design and operation of fast reactors. The measurements were performed with quasi-monoenergetic neutrons at TUNL, and special care has been taken to obtain high-quality data with minimum associated uncertainties. The

cross-section data were compared with data and the latest evaluations from the literature. Statistical-model calculations were carried out based on the Hauser-Feshbach formalism using the CoH₃ code and were found to be in very good agreement with the present data. Our future plans include measurements of the $^{238}\text{U}(n,\gamma)^{239}\text{U}$ cross section, although the capture reaction channel is by far the smallest in this high-energy region.

ACKNOWLEDGMENTS

We wish to thank M. B. Chadwick (LANL) for his insight and support for the present measurements. This work was supported in part by the National Nuclear Security Administration (NNSA) under the Stewardship Science Academic Alliances Program through the US Department of Energy, Grant No. DE-NA0002936, and the US Department of Energy, Office of Nuclear Physics, under Grant No. DE-FG02-97ER41033, and by Lawrence Livermore National Laboratory, operated by the Lawrence Livermore National Security, LLC under Contract No. DE-AC52-07NA27344, and by Los Alamos National Laboratory, operated by the Los Alamos National Security, LLC under Contract No. DE-AC52 06NA25396.

-
- [1] C. Wagemans, *The Nuclear Fission Process* (CRC Press, Boca Raton, FL, 1991).
- [2] R. C. Haight, M. B. Chadwick, and D. J. Vieira, *Los Alamos Science* **30**, 52 (2006).
- [3] S. Pelloni, G. Youinou, and P. Wydler, *Proceedings of the International Conference of Nuclear Data for Science and Technology, Trieste, Vol. 59, part-II, p. 1172* (1997).
- [4] J. A. Phillips, Report No. AERE-NP/R-2033 (1956).
- [5] G. P. Antropov, Yu. A. Zysin, A. A. Kovrizhnykh, and A. A. Lbov, *J. Sov. At. Energy* **5**, 1352 (1958).
- [6] J. D. Knight, R. K. Smith, and B. Warren, *Phys. Rev.* **112**, 259 (1958).
- [7] J. L. Perkin and R. F. Coleman, *J. Nucl. Energy (Part A and B)* **14**, 69 (1961).
- [8] D. S. Mather and L. F. Pain, *Phys. Rev.* **133**, B1403 (1964).
- [9] D. S. Mather, P. F. Bampton, R. E. Coles, G. James, and P. J. Nind, Report: A. W. R. E. Aldermaston Reports, No. 72/72, UK (1972).
- [10] J. H. Landrum, R. J. Nagle, and M. Lindner, *Phys. Rev. C* **8**, 1938 (1973).
- [11] L. R. Veaser and E. D. Arthur, in *Proceedings of the International Conference on Neutron Physics and Nuclear Data for Reactors and Other Applied Purposes, Harwell, England* (OECD Nuclear Energy Agency, Paris, 1978), p. 1054.
- [12] H. Karius, A. Ackermann, and W. Scobel, *J. Phys. G* **5**, 715 (1979).
- [13] N. V. Kornilov, B. V. Zhuravlev, O. A. Sal'nikov, P. Raics, S. Nagy, S. Daroczy, K. Sailer, and J. Csikai, Zentralinstitut für Kernforschung (ZFK), Rossendorf, Germany Report No. 410, p. 68 (1980).
- [14] T. B. Ryves and P. Kolkowski, *J. Phys. G* **6**, 771 (1980).
- [15] J. Frehaut, A. Bertin, R. Boris, and J. Jary, Report No. INDC(USA) **84**, 399 (1980), <https://www-nds.iaea.org/publications/indc/indc-usa-0084-vol1/>; J. Frehaut, A. Bertin, and R. Bois, *Nucl. Science Eng.* **74**, 29 (1980).
- [16] P. Raics, S. Nagy, S. Daroczy, J. Csikai, N. V. Kornilov, B. V. Zhuravlev, and O. A. Salnikov, Report No. INDC(HUN) **17**, 47 (1980), <https://www-nds.iaea.org/publications/indc/indc-hun-0017/>.
- [17] B. Anders, B. M. Bahal, and R. Pepelnik, Report GKSS-85-E-24 (1985), <https://www.nndc.bnl.gov/exfor/servlet/X4sGetSubent?reqx=55308&subID=21976048>; R. Pepelnik, B. Anders, B. M. Bahal, and M. Farooq, Report INDC(GER) **28**, 32 (1986), <https://www-nds.iaea.org/publications/indc/indc-ger-0028/>.
- [18] V. YA. Golovnya, K. S. Goncharov, G. P. Dolya, V. A. Kuz'menko, S. G. Pasechnik, and V. V. Remaev, Report KIEV **3**, 281 (1987).
- [19] P. Raics, S. Nagy, S. Daroczy, and N. V. Kornilov, Report No. INDC(HUN), Vol. 29, 3 (1990), <https://www-nds.iaea.org/publications/indc/indc-hun-0029/>.
- [20] C. Konno, Y. Ikeda, K. Oishi, K. Kawade, H. Yamamoto, and H. Maekawa, Report No. JAERI-1329 (1993).
- [21] X. Wang, Shan Jiang, Ming He, Kejun Dong, and Caijing Xiao, *Nucl. Instrum. Methods Phys. Res. A* **621**, 326 (2010); X. Wang, S. Jiang, Ming He, Guozhu He, Chaoli Li, Shizhou Li, Jie Gong, and L. Lu, *Nucl. Instrum. Methods Phys. Res. B* **268**, 1949 (2010).
- [22] C. Zhu, Y. Chen, Yunfeng Mou, Pu Zheng, T. He, X. Wang, Li An, and H. Guo, *Nucl. Sci. Eng.* **169**, 188 (2011).
- [23] H. Naik, S. V. Suryanarayana, V. K. Mulik, P. M. Prajapati, B. S. Shivashankar, K. C. Jagadeesan, S. V. Thakare, D. Raj, S. C. Sharma, P. V. Bhagwat, S. D. Dhole, S. Ganesan, V. N. Bhoraskar, and A. Goswami, *J. Radioanal. Nucl. Chem.* **293**, 469 (2012).

- [24] R. Crasta, S. Ganesh, H. Naik, A. Goswami, S. V. Suryanarayana, S. C. Sharma, P. V. Bhagwat, B. S. Shivashankar, V. K. Mulik, and P. M. Prajapati, *Nucl. Sci. Eng.* **178**, 66 (2014).
- [25] V. K. Mulik, S. V. Suryanarayana, H. Naik, S. Mukerji, B. S. Shivashankar, P. M. Prajapati, S. D. Dhole, V. N. Bhoraskar, S. Ganesan, and A. Goswami, *Ann. Nucl. Energy* **63**, 233 (2014).
- [26] H. Naik, S. V. Suryanarayana, S. Bishnoi, T. Patel, A. Sinha, and A. Goswami, *J. Radioanal. Nucl. Chem.* **303**, 2497 (2015).
- [27] A. A. Filatenkov, INDC(CCP)-0460 Rev. Distr. G+J, 2016; A. A. Filatenkov, S. V. Chuvaev, V. N. Aksenov, V. A. Yakovlev, A. V. Malyshev, S. K. Vasil'ev, M. Avrigeanu, V. Avrigeanu, D. L. Smith, Y. Ikeda, A. Wallner, W. Kutschera, A. Priller, P. Steier, H. Vonach, G. Mertens, and W. Rochow, Report Nos. RI-252 (1999) and INDC(CCP)-402, 1997.
- [28] www.nndc.bnl.gov.
- [29] K. I. Zolotarev, INDC(NDS)-0741, Distr. AD/G/IN/J/RD, August 2017.
- [30] www.tunl.duke.edu.
- [31] C. Bhatia, B. Fallin, M. E. Gooden, C. R. Howell, J. H. Kelley, W. Tornow, C. W. Arnold, E. M. Bond, T. A. Bredeweg, M. M. Fowler, W. A. Moody, R. S. Rundberg, G. Rusev, D. J. Vieira, J. B. Wilhelmy, J. A. Becker, R. Macri, C. Ryan, S. A. Sheets, M. A. Stoyer, and A. P. Tonchev, *Nucl. Instrum. Methods Phys. Res. A* **757**, 7 (2013).
- [32] D. E. González Trotter, F. Salinas Meneses, W. Tornow, A. S. Crowell, C. R. Howell, D. Schmidt, and R. L. Walter, *Nucl. Instrum. Methods Phys. Res. A* **599**, 234 (2009).
- [33] M. E. Gooden, C. W. Arnold, J. A. Becker, C. Bhatia, M. Bhide, E. M. Bond, T. A. Bredeweg, B. Fallin, M. M. Fowler, C. R. Howell, J. H. Kelley, Krishichayan, R. Macri, G. Rusev, C. Ryan, S. A. Sheets, M. A. Stoyer, A. P. Tonchev, W. Tornow, D. J. Vieira, and J. B. Wilhelmy, *Nucl. Data Sheets* **131**, 319 (2016).
- [34] M. Drog, *Nucl. Sci. Eng.* **67**, 190 (1978).
- [35] www.canberra.com.
- [36] Eckert and Ziegler, www.ezag.com/home/products/isotope-products.html.
- [37] D. C. Radford, *Nucl. Instrum. Methods Phys. Res. A* **361**, 297 (1995).
- [38] B. Champine, M. E. Gooden, Krishichayan, E. B. Norman, N. D. Scielzo, M. A. Stoyer, K. J. Thomas, A. P. Tonchev, W. Tornow, and B. S. Wang, *Phys. Rev. C* **93**, 014611 (2016).
- [39] R. Raut, A. S. Crowell, B. Fallin, C. R. Howell, C. Huijbregtse, J. H. Kelley, T. Kawano, E. Kwan, G. Rusev, A. P. Tonchev, W. Tornow, D. J. Vieira, and J. B. Wilhelmy, *Phys. Rev. C* **83**, 044621 (2011).
- [40] A. P. Tonchev, C. T. Angell, M. Boswell, A. S. Crowell, B. Fallin, S. Hammond, C. R. Howell, A. Hutcheson, H. J. Karwowski, J. H. Kelley, R. S. Pedroni, W. Tornow, J. A. Becker, D. Dashdorj, J. Kenneally, R. A. Macri, M. A. Stoyer, C. Y. Wu, E. Bond, M. B. Chadwick, J. Fitzpatrick, T. Kawano, R. S. Rundberg, A. Slemmons, D. J. Vieira, and J. B. Wilhelmy, *Phys. Rev. C* **77**, 054610 (2008).
- [41] K. I. Zolotarev, International Nuclear Data Committee Report No. INDC(NDS)-0526, Dist. RD Aug (2008).
- [42] K. I. Zolotarev, International Nuclear Data Committee Report No. INDC(NDS)-0546, Dist. RD April (2009).
- [43] T. Kawano, P. Talou, M. B. Chadwick, and T. Watanabe, *J. Nucl. Science Technology* **47**, 462 (2010).
- [44] C. A. Engelbrecht and H. A. Weidenmüller, *Phys. Rev. C* **8**, 859 (1973).
- [45] T. Kawano, R. Capote, S. Hilaire, and P. Chau Huu-Tai, *Phys. Rev. C* **94**, 014612 (2016).
- [46] F. S. Dietrich, I. J. Thompson, and T. Kawano, *Phys. Rev. C* **85**, 044611 (2012).
- [47] E. Sh. Soukhovitskii, R. Capote, J. M. Quesada, and S. Chiba, *Phys. Rev. C* **72**, 024604 (2005).
- [48] P. Möller, J. R. Nix, W. D. Myer, and W. J. Swiatecki, *At. Data Nucl. Data Tables* **59**, 185 (1995).
- [49] J. Kopecky and M. Uhl, *Phys. Rev. C* **41**, 1941 (1990).
- [50] R. Capote, M. Herman, P. Obložinský, P. G. Young, S. Goriely, T. Belgia, A. V. Ignatyuk, A. J. Koning, S. Hilaire, V. A. Plujko, M. Avrigeanu, O. Bersillon, M. B. Chadwick, T. Fukahori, Z. Ge, Y. Han, S. Kailas, J. Kopecky, V. M. Maslov, G. Reffo, M. Sin, E. Sh Soukhovitskii, and P. Talou, *Nucl. Data Sheets* **110**, 3107 (2009).
- [51] J. L. Ullmann, T. Kawano, T. A. Bredeweg, A. Couture, R. C. Haight, M. Jandel, J. M. O'Donnell, R. S. Rundberg, D. J. Vieira, J. B. Wilhelmy, J. A. Becker, A. Chyzh, C. Y. Wu, B. Baramsai, G. E. Mitchell, and M. Krtička, *Phys. Rev. C* **89**, 034603 (2014).
- [52] S. L. Hammond, A. S. Adekola, C. T. Angell, H. J. Karwowski, E. Kwan, G. Rusev, A. P. Tonchev, W. Tornow, C. R. Howell, and J. H. Kelley, *Phys. Rev. C* **85**, 044302 (2012).